

## VESICLE NUMBER DOES NOT PREDICT POSTSYNAPTIC MEASURES OF MINIATURE SYNAPTIC ACTIVITY FREQUENCY IN CULTURED CORTICAL NEURONS

P. J. MACKENZIE,\* G. S. KENNER,\* O. PRANGE\* and T. H. MURPHY\*†‡

Kinsmen Laboratory of Neurological Research, Departments of \*Psychiatry and †Physiology, University of British Columbia, Vancouver, BC, Canada, V6T 1Z3

**Abstract**—We tested the hypothesis that heterogeneity in the frequency of miniature synaptic activity reflects differences in the number of vesicles present in presynaptic terminals. Using imaging techniques, we measured dendritic miniature synaptic calcium transients attributed to the spontaneous release of single transmitter quanta. Following imaging, the identified neurons were processed for serial transmission electron microscopy. At sites of quantal  $\text{Ca}^{2+}$  transients mediated by *N*-methyl-D-aspartate receptors, we confirmed the presence of excitatory synapses and measured the total number of vesicles and the number of docked vesicles.

We observed no correlation between the frequency of spontaneous miniature activity and either the total vesicle number or the number of docked vesicles. We conclude that the presynaptic vesicle complement as measured by ultrastructural analysis does not necessarily determine the frequency of spontaneous activity at synapses mediated by *N*-methyl-D-aspartate receptors. © 2000 IBRO. Published by Elsevier Science Ltd. All rights reserved.

**Key words:** NMDA, quantal, EPSC, release, ultrastructure, electron microscopy.

Studies using electron microscopy (EM) have indicated that the morphology of cortical excitatory glutamatergic synapses is highly variable.<sup>19</sup> Bouton size, vesicle number, vesicle diameter and postsynaptic spine volume vary widely within a relatively homogenous population of neurons.<sup>36,41</sup> It has been hypothesized that structural differences between synapses underlie some of the functional differences that are observed between neurons.<sup>6,11,24</sup> Accordingly, it is necessary to assess both synaptic structure and function at single CNS synapses.

We have recently described techniques to compare structure and function at multiple synapses along a region of dendrite.<sup>26</sup> Using  $\text{Ca}^{2+}$  imaging, we measured the *N*-methyl-D-aspartate (NMDA) receptor-mediated component of spontaneous miniature excitatory postsynaptic currents (mEPSCs), termed the miniature synaptic  $\text{Ca}^{2+}$  transient (MSCT).<sup>31,32</sup> Calcium imaging provides a method to localize synaptic responses to particular dendritic spines.<sup>29,31,34</sup> Sensitivity to the NMDA receptor antagonist D,L-APV suggested that under the conditions we have used,  $\text{Ca}^{2+}$  transients associated with miniature synaptic activity are largely attributed to NMDA receptors.<sup>31,48,34</sup> We have previously reported a positive correlation between the MSCT amplitude and mEPSC amplitude,<sup>32</sup> indicating that  $\text{Ca}^{2+}$  imaging can be used to evaluate the local characteristics of synaptic events. Following MSCT imaging, we performed serial reconstruction of transmission EM images to identify synapses at the origins of the  $\text{Ca}^{2+}$  transients. This enabled the ultrastructural characterization of the specific synapses where MSCTs were

measured. Using these techniques, we have previously reported that synapse size correlated positively with the amplitude of the NMDA component of the quantal postsynaptic response, suggesting that synapse size may place a limit on the number of postsynaptic receptors.<sup>26</sup>

In the present report, we explore the relationship between MSCT frequency and the ultrastructure of the presynaptic terminals. We report that the number of vesicles present in a presynaptic terminal does not correlate with MSCT frequency. Furthermore, we find no relationship between MSCT frequency and the number of docked vesicles. Therefore, the frequency of miniature activity is controlled by other factors at these synapses; we discuss alternative possibilities.

### EXPERIMENTAL PROCEDURES

The experimental procedures have been described in detail previously.<sup>26</sup> In brief, cortical neurons and glia were dissociated from 17–18 day gestation Wistar rat fetuses, placed in culture and allowed to mature for 17–26 days *in vitro*. All experiments strictly followed the Canadian Council on Animal Care guidelines; the protocols used were approved by the Committee on Animal Care (The University of British Columbia; animal care certificate A95-0296). Whole cell patch clamp recordings were used to load neurons with the fluorescent dyes fluo-3 and fura-2. The patch pipette solution contained (in mM): 3–5 fluo-3  $\text{K}^+$  salt, 5 fura-2  $\text{K}^+$  salt (relatively  $\text{Ca}^{2+}$  insensitive and used to view basal fluorescence), 92  $\text{KMeSO}_4$ , 20  $\text{NaCl}$ , 5  $\text{Mg-ATP}$ , 0.3  $\text{GTP}$ , 10  $\text{HEPES}$ , and 0.3–0.8%  $\text{Biocytin HCl}$  (pH = 7.3; 280 mOsm; adjusted with  $\text{KMeSO}_4$ ). After neurons were loaded (about 2–4 min of perfusion), the electrode was removed and the cells were allowed to recover in the presence of 0.3  $\mu\text{M}$  tetrodotoxin (TTX) containing saline for 1–2 h. The following extracellular solution was used to measure the  $\text{Ca}^{2+}$  component of mEPSCs (in mM): 137  $\text{NaCl}$ , 5  $\text{KCl}$ , 5  $\text{CaCl}_2$ , 0  $\text{MgCl}_2$ , 0.34  $\text{Na}_2\text{HPO}_4(7\text{H}_2\text{O})$ , 10  $\text{Na HEPES}$ , 22  $\text{glucose}$ , 1  $\text{NaHCO}_3$ , 0.2  $\mu\text{M}$  picrotoxin, 0.0003  $\text{TTX}$ , pH 7.4.<sup>31</sup>

### Imaging and analysis

Imaging was performed with a 100× 1.3 NA Zeiss objective on a

†To whom correspondence should be addressed.

E-mail address: thmurphy@unixg.ubc.ca (T. H. Murphy).

**Abbreviations:** AMPA, D,L-alpha-amino-3-hydroxy-isoxazole propionate; APV, D,L-amino-5-phosphono-valeric acid; DPBS, Dulbecco's phosphate-buffered saline; EM, electron microscopy; EPSC, excitatory postsynaptic current; HEPES, *N*-2-hydroxyethylpiperazine-2-ethanesulfonic acid; MSCT, miniature synaptic  $\text{Ca}^{2+}$  transient; NMDA, *N*-methyl-D-aspartate; RT, room temperature; SD, standard deviation; TTX, tetrodotoxin.

Zeiss Axiovert microscope with a stage that permitted movement during patch clamp recording. A fiberoptically coupled intensified CCD camera (Stanford Photonics, Palo Alto, CA, U.S.A.) with a Gen III intensifier tube was used for widefield image acquisition (33 ms temporal resolution). For frame grabbing an Epix 4M12-64 MB board (Northbrook, IL, U.S.A.) was used. For each experiment, 300 images of fluo-3 fluorescence were collected in 10-s sweeps (up to 17 sweeps per experiment) and were analysed offline using IDL (Research Systems, Boulder, CO, U.S.A.).

To view processes under baseline conditions and to correct for process volume and cell loading (see below), the fluorescent  $\text{Ca}^{2+}$  indicator fura-2 (excitation 380 nm) was co-injected with fluo-3 (excitation 480 nm). Fura-2 was chosen for its high fluorescence signal at basal  $[\text{Ca}^{2+}]_i$ , its low affinity for  $\text{Ca}^{2+}$  with little attendant buffering, and its distinctive spectrum that did not contaminate fluo-3 signals. A single fura-2 image (average of 30 images acquired over 1 s) was taken for every trial following 10 s of fluo-3 calcium imaging. The fura-2 signal was corrected for autofluorescence by subtracting the average background pixel value (adjacent to a dendritic region). Background fluorescence was highly stable and did not exhibit rapid changes which resemble those during MSCTs. Measurement boxes ( $1.4\text{--}2\ \mu\text{m}^2$ ) were placed over the fura-2 image of a spine or dendrite of interest, and boxes with the identical coordinates were used for analysis of fluo-3 fluorescence changes ( $\Delta F_{480}$ ). Fluo-3 fluorescence signals were considered miniature synaptic calcium transients (MSCTs) if at least four consecutive measurements were 1 standard deviation (SD) above baseline fluo-3 fluorescence. The MSCT initiation time was defined as the first point above baseline; the initiation site of the MSCT was identified by the earliest rise in fluorescence. In almost all cases, the site of MSCT initiation was associated with a clear morphological feature such as a varicosity or spine.  $\text{Ca}^{2+}$  responses were calculated for individual trials within  $1.4\text{--}2.0\ \mu\text{m}^2$  regions surrounding sites of MSCT origin (spines).  $\text{Ca}^{2+}$  responses were quantified by measuring the change in fluo-3 fluorescence ( $\Delta F_{480}$ ) scaled to spine volume ( $F_{380}$ ; basal fura-2 fluorescence) as previously described in detail.<sup>26</sup>

### Electron microscopy

Following MSCT imaging, preparations were fixed with 4% paraformaldehyde and 0.2–0.5% glutaraldehyde in 0.1 M Sørensen's  $\text{Na}^+$  phosphate buffer (pH 7.2–7.4, 1.5 h, room temperature (RT)), rinsed briefly in Dulbecco's phosphate-buffered saline (DPBS), permeabilized in 0.1–0.2% Triton X-100 in DPBS (3–4 min, RT), washed with DPBS (3–5 volumes over 5 min, RT) and blocked in 2.5% normal goat serum in DPBS (4–12 h, 48°C). Specimens were then washed with DPBS (3–5 volumes over 30 min, RT), incubated with Vector Labs A/B reagent (avidin/biotinylated peroxidase complex; 1 h, RT), washed with DPBS (3–5 volumes over 30 min, RT), and incubated in 0.5 mg/ml diaminobenzidine (DAB) and 0.015%  $\text{H}_2\text{O}_2$  in DPBS for 2–5 min (RT; intensity monitored to prevent over-staining). DPBS washing (5 volumes over at least 30 min, RT) was followed by further fixation in 2.5% glutaraldehyde in 0.1 M Sørensen's buffer (pH 7.2–7.4, 1 h, on ice), washing in the same buffer (3 volumes over 30 min, on ice). Preparations were then postfixed in 1%  $\text{OsO}_4$  in the same buffer (1 h, on ice). Following a final Sørensen's buffer wash (3 volumes over 30 min, on ice), cultures were dehydrated in a graded ethanol series (50, 70, 85, 95, 100%) and flat embedded in Spurr resin on Aclar plastic (Proplastics, Linden, NJ, U.S.A.). Following polymerization, areas containing single stained neurons were excised, separated from the Aclar and mounted on blank blocks. Serial sections of  $\sim 70$  nm thickness were collected on pioloform or Formvar-coated single slot grids, stained with 3% aqueous uranyl acetate (UA) or 5% UA in 20% MeOH, followed by lead citrate, then examined at 80 keV in a Zeiss EM 10°C STEM. A montage of low-power electron micrographs (8000 $\times$ ) was aligned with fluorescence and bright-field images. From this overlay, it was possible to identify DAB-stained dendritic spines where MSCT events had occurred. Staining selectivity arises since both the  $\text{Ca}^{2+}$  indicators and biocytin are injected into a single neuron.

Analysis of the serial electron micrographs was used to reconstruct 20 synapses from four neurons. Synapses were identified by the presence of pre- and postsynaptic membrane apposition, synaptic cleft thickening, a presynaptic para-membranous density, and clustering of at least three vesicles near the presynaptic membrane. Synapse volume was measured by tracing outlines of consecutive EM sections

through the synaptic compartment of interest and multiplying each area enclosed in the outline by the thickness of the optical section (70 nm). Of the 20 synapses analysed, two were shaft synapses; spine volume was therefore measured at the remaining 18 spines (12 single macular synapses, four perforated synapses with the same pre-synaptic bouton, and two spines each contacting two presynaptic boutons). In many cases the intensity of the DAB staining prevented accurate measurement of the postsynaptic density size. Therefore we measured the synaptic contact area defined as the region of increased (and relatively constant) thickness between the apposed pre- and postsynaptic membranes. At seven of the 20 synapses, the synaptic contact area was not measurable throughout its full extent due to a tangential plane of section. Synaptic contact area was therefore analysed at the remaining 13 synapses. These included two perforated synapses (with two separate clusters of vesicles from the same pre-synaptic bouton), in which the area of the perforation was included in the measurement of synaptic contact area. Perforated synapses with more than one presynaptic bouton ( $n=3$ ) were excluded from the analysis.

Presynaptic vesicles were counted at the 17 synapses containing only one presynaptic bouton. Counts were made from all serial EM contact prints without knowledge of the corresponding physiological data: consistency between two observer was  $>95\%$ . As the total number of vesicles was quantified within the entire volume of the synapse, application of unbiased counting procedures, such as the disector method, were not required. A vesicle was counted in a given section if its electron-dense perimeter (membrane) was visibly surrounded by a lighter core. While this method may potentially lead to an overestimation of vesicle number due to duplicate counting of a given vesicle in two adjacent sections this error should be consistent at all synapses. Additionally, the section thickness (70 nm) was greater than the vesicle size, suggesting that the error was small.<sup>10</sup> Vesicle profiles were occasionally unobtainable due to section folding. In such cases, vesicle number was estimated by linear interpolation between adjacent sections; data were used only if the amount estimated accounted for less than 10% of spine volume. The addition of estimated data did not appreciably change the correlations that were obtained. Since relative spine size (scaled to the mean spine size for each specimen) was correlated with MSCT frequency, no correction was applied for differential shrinkage in the Z-dimension during ethanol dehydration.<sup>45</sup> In some specimens detergents required in the staining process degraded the ultrastructure.

### Confocal microscopy

In addition to EM, confocal microscopy was used for morphological analysis of spines following fluorescence imaging of MSCTs as described above. In these cases cells were fixed with 4% paraformaldehyde in 0.1 M Sørensen's buffer (pH 7.2–7.4, 1.5 h, RT) rinsed briefly in DPBS, permeabilized in 0.2–0.5% Triton X-100 in DPBS (4–5 min, RT), washed with DPBS (3–5 volumes over 5 min, RT) and blocked in 1.5–2.5% normal goat serum in DPBS (4–12 h, 4°C). Cultures were washed with DPBS (3–5 volumes over 30 min, RT), incubated with 20  $\mu\text{g}/\text{ml}$  avidin–fluorescein in DPBS (Vector; 1–2 h, RT), washed with DPBS (3–5 volumes over 30 min, RT) and mounted on a slide with Antifade in glycerol/DPBS (Molecular Probes, Eugene, OR, U.S.A.). Confocal imaging was performed with a Bio-Rad MRC 600 system attached to a Zeiss Axioskop microscope and a  $100\times 1.3$  NA Zeiss objective. Serial images (step size  $0.54\ \mu\text{m}$ ) along the z-axis (z-series) were obtained through the dendritic region of interest and a maximal-intensity projection was used to generate a two-dimensional representation of the spines. A maximal intensity projection flattens three-dimensional images by creating an image of the maximal pixel value for each pixel across the sections. In order for a spine to be selected for measurement, it was necessary to resolve clearly at least one MSCT event initiated at the spine. Since a wide field CCD camera used for MSCT imaging has a lower resolution than a confocal microscope, it was a limiting factor in identifying spines. Therefore, our study was restricted to relatively larger and well-defined spines.<sup>44</sup> Spines that were selected could be clearly resolved from other structures in the maximal-intensity confocal projection image; at least two rows of pixels of lower intensity were between two adjacent spines or between spine head and dendrite. Cross-sectional spine area was quantified using NIH image and Adobe Photoshop.

For statistical analyses, the non-parametric Spearman test was used; the significance level was set to 0.05.

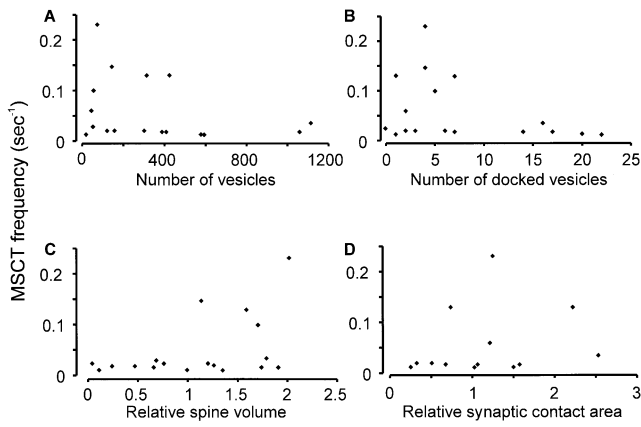


Fig. 1. The relationship between MSCT frequency and synapse structural parameters. The frequency of NMDA receptor dependent quantal miniature synaptic  $\text{Ca}^{2+}$  transients (MSCTs), as determined by  $\text{Ca}^{2+}$  imaging, was assessed for 17 confirmed single synapses from four cortical neurons. (A) MSCT frequency plotted versus number of vesicles at single synapses. No significant correlation was observed (Spearman  $r = -0.31$ ,  $P > 0.05$ ). (B) MSCT frequency plotted versus number of docked vesicles (Spearman  $r = -0.41$ ,  $P > 0.05$ ). (C) MSCT frequency versus relative spine volume (Spearman  $r = 0.28$ ,  $P > 0.05$ ). (D) MSCT frequency versus relative synaptic contact area (Spearman  $r = 0.30$ ,  $P > 0.05$ ).

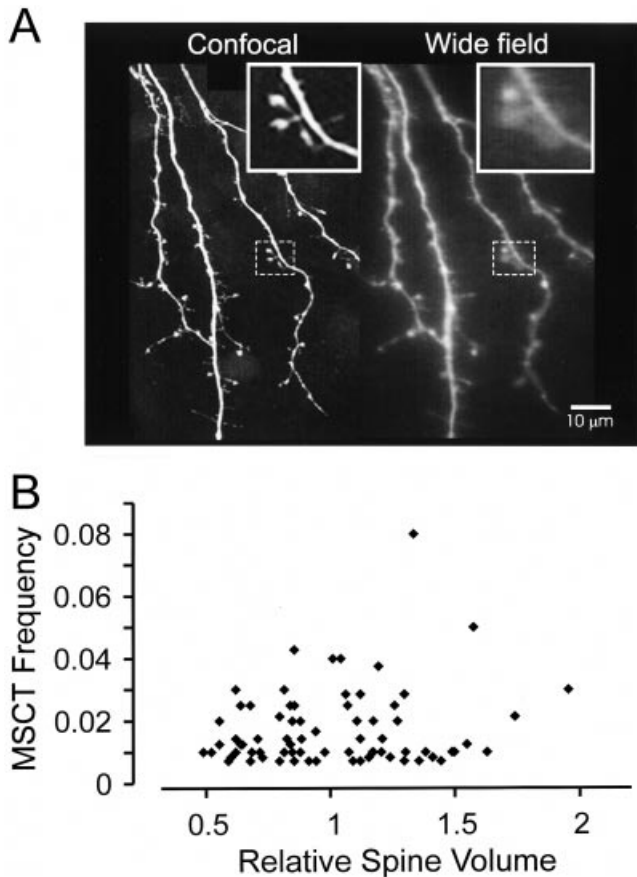


Fig. 2. The relationship between MSCT frequency and confocal measurement of spine size. (A) Example of confocal analysis of dendritic structure versus wide field image used for MSCT frequency calculation. (B) MSCT frequency plotted versus spine volume (scaled to mean for each experiment) for 74 spines from five cortical neurons. No significant correlation was observed (Spearman  $r = 0.07$ ,  $P > 0.05$ ).

## RESULTS

### *Calcium imaging and parallel ultrastructural analysis of single synapses*

We have conducted experiments designed to assess both structure and function at the same CNS synapses. Cultured cortical neurons were injected with fluo-3 and imaging of miniature synaptic calcium transient (MSCTs) was used to map quantal synaptic responses to identified dendritic regions. Co-injection of biocytin allowed the selective staining of the neuron of interest following MSCT imaging. The combined use of MSCT imaging and serial EM reconstruction enabled the comparison of quantal responses at morphologically identified CNS synapses as previously described.<sup>26</sup>

### *Miniature $\text{Ca}^{2+}$ transient frequency is not correlated with number of synaptic vesicles*

Previous studies performed in this laboratory indicate that miniature release rates can vary widely between synapses and are not described by a Gaussian distribution.<sup>31,48</sup> To identify factors that may contribute to the skewed distribution of miniature frequency, we measured the probability of spontaneous activity using MSCT imaging and subsequently counted the number of vesicles at the same synapses. We observed no significant correlation between the total number of vesicles and MSCT frequency (Spearman  $r = -0.31$ ,  $P > 0.05$ ; Fig. 1A) or between relative vesicle number and relative frequency (scaled to the mean of each experiment;  $r = 0.05$ ,  $P > 0.05$ ). Furthermore, no correlation was obtained between the number of vesicles docked at the presynaptic membrane and MSCT frequency ( $r = -0.41$ ,  $P > 0.05$ ; Fig. 1B).

Additional parameters of synaptic structure such as spine volume and synaptic contact area failed to show simple linear relationships with miniature response frequency (Fig. 1C, D). Analysis using a non-parametric Spearman rank-order test also revealed no significant correlation between MSCT frequency and spine volume, and between MSCT frequency and synaptic contact area ( $P > 0.05$ ).

To further test the relationship between synaptic structure and miniature frequency we have used confocal microscopy to measure synapse size (Fig. 2A). In these experiments neurons were also injected with a combination of biocytin and  $\text{Ca}^{2+}$  indicators.<sup>26</sup> MSCT imaging was performed to determine response frequency at 74 spines from five neurons. Using this pooled data set we observed no relationship between response frequency and relative synapse size determined from a confocal projection image (Spearman  $r = 0.07$ ,  $P > 0.05$ ; Fig. 2B).

Recent work<sup>33</sup> suggests that spontaneous release rates for hippocampal synapses may be quite low, 0.002 releasable vesicles/s per synapse. Given that there may be about five vesicles within a readily releasable pool this results in an expected release rate of approximately 0.01/s per synapse.<sup>33</sup> We observed that some synapses had MSCT rates that were more than ten times higher than others. To assess if these synapses represent a distinct subpopulation we examined whether the distribution of MSCTs rates was significantly skewed or was bimodal due to the presence of these synapses. Analysis of the release rate distribution (across synapses) indicated a skew towards synapses with high release rates as observed previously in this system.<sup>48</sup> No evidence was

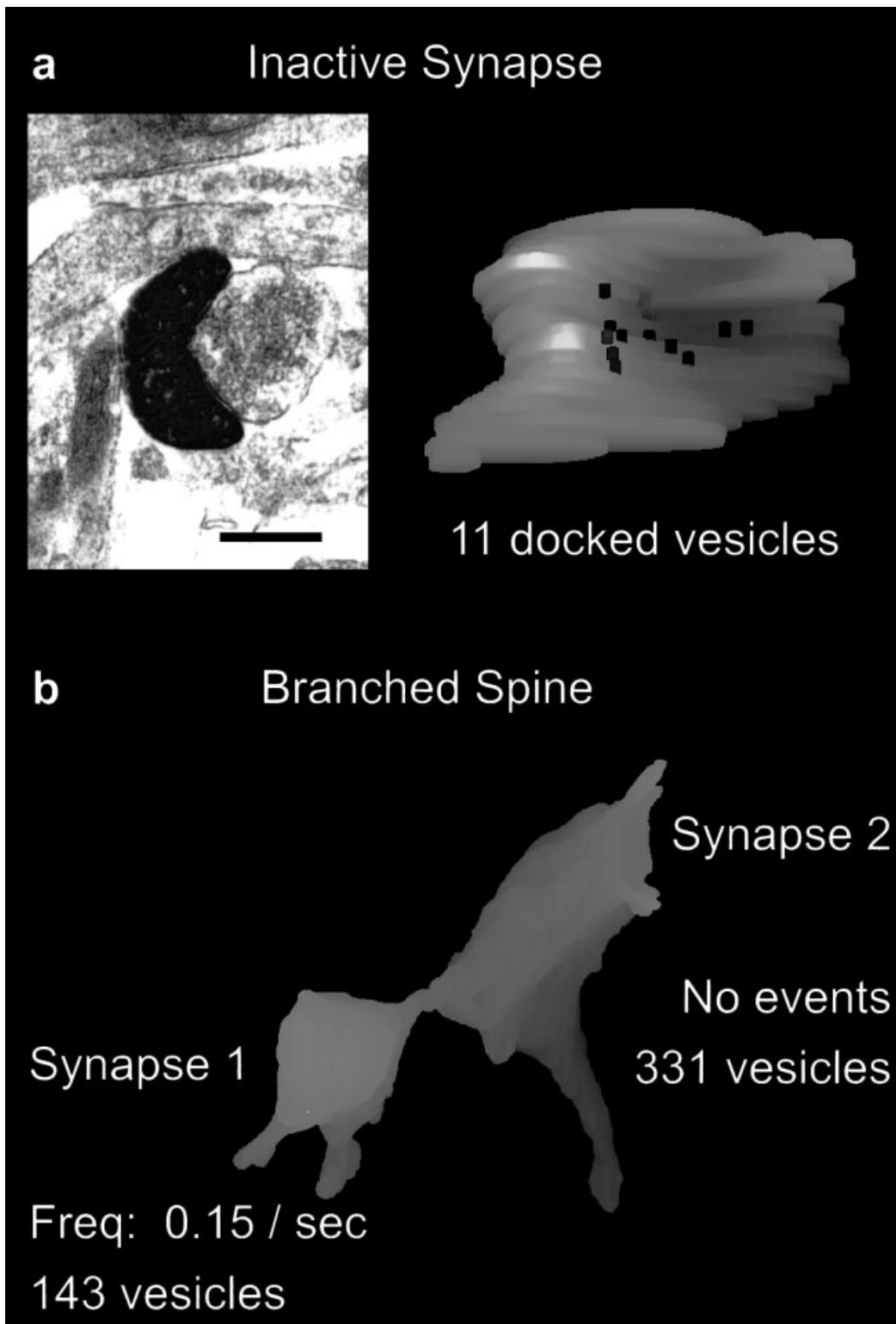


Fig. 3. Three-dimensional reconstruction of sites with different miniature release frequencies. (a) Left panel: electron micrograph illustrating a cross-section through a synapse that exhibited no MSCT events. The spine is indicated by the DAB-stained material; a presynaptic terminal with vesicles is evident. Scale bar = 0.4  $\mu\text{m}$ . Right panel: serial EM reconstruction confirms a single release site with 11 docked vesicles as indicated by the dark circles. (b) A branched spine illustrating two adjacent synapses  $< 2 \mu\text{m}$  apart with widely different release probability. Synapse 1 was a highly active site, while synapse 2 was inactive, yet contained more vesicles.

found for a bimodal distribution. Within the relatively small EM data set, we found that exclusion of synapses with high rates of MSCTs ( $>0.05/\text{s}$ ) removed the positive skew and resulted in a normally distributed population of release

rates. However, exclusion of synapses with considerably higher release rates ( $>0.05$  MSCTs/s) did not improve the correlation between ultrastructural measures of presynaptic terminal size such as vesicle number, synapse volume, and

docked vesicle number and the frequency of MSCTs (data not shown). In the case of confocal analysis of synapse size, synapses with elevated release rates (0.03 or 0.05 MSCTs/s) were also excluded from correlation between confocal measurement of synapse size and MSCT rates. Without these synapses a skew in release rates was still observed and the correlation between MSCT rate and synapse area was not improved.

*Apparently inactive synapses show normal ultrastructure with docked vesicles*

We have observed (>10) synapses with excitatory synapse morphology (asymmetrical synapses at spines) showing no spontaneous release yet containing docked, presumably releasable, vesicles. For example, the synapse illustrated in Fig. 3a included 11 docked vesicles and 234 total vesicles, yet no spontaneous release was observed at this synapse, indicating that the docked state (defined morphologically) can be stable.<sup>33</sup> Of the 20 synapses that we reconstructed, we found one example of an apparently branched spine in which two synapses were within 2  $\mu\text{m}$  of each other. The three-dimensional reconstruction of this spine from serial EM sections is illustrated in Fig. 3b. Synapse 1, the smaller synapse (143 vesicles), showed a high MSCT rate (0.15/s; 26 events) while the adjacent larger synapse 2 (331 vesicles) did not exhibit any MSCTs during 170 s of image acquisition. Thus, the frequency of miniature transients can vary greatly between adjacent portions of branched spines, apparently independently of their vesicle status or content.

## DISCUSSION

It has been widely hypothesized that alterations in synapse structure underlie changes in synapse efficacy.<sup>11,24</sup> Many experiments have reported structural changes in synaptic populations following manipulations of synaptic strength or following learning<sup>8,12,13,18,22,27,30,35,40,42</sup> (but see Ref. 43). Unlike population studies, we have directly compared structure and function at the same synapses. Previous studies<sup>14</sup> have used ultrastructural analysis in combination with patch clamp of single mammalian CNS boutons, although the functional and structural parameters of multiple synapses were not compared.

Experiments in invertebrates indicate that synaptic strength is correlated with the number of synaptic vesicles and synapse size.<sup>4</sup> Structure–function correlations have also been identified in crustacean motor neurons.<sup>7,49</sup> Accordingly, we have measured both the probability of spontaneous activity (MSCT frequency) and the vesicle number in identified mammalian CNS synapses. At synapses reconstructed from serial transmission EM, we observed no correlation between MSCT frequency and either the number of docked vesicles, the total number of vesicles, spine size or synaptic contact area (Fig. 1). Consistent results were obtained using confocal imaging to measure spine volume (Fig. 2). Furthermore, we frequently observed presumed excitatory synapses with many apparently docked vesicles (up to 11) that showed no miniature activity over  $\sim 3$  min (Fig. 3a). These findings contrast with a recent hypothesis that the readily releasable pool, which determines action potential-evoked release probability, may be equivalent to the number of docked vesicles.<sup>9,38,41</sup> These results, although preliminary, suggest that miniature

release probability may be controlled by factors in addition to the number of morphologically docked vesicles. Conceivably, vesicles that are subject to spontaneous release may represent a subset of the morphologically docked vesicles that have been further “primed” through a mechanism that cannot currently be resolved at the ultrastructural level.<sup>16</sup> Observations that miniature release rates can vary by more than 10-fold between synapses would argue that release probability is not merely determined by the number of available release sites. Alternatively, miniature release rate may be controlled by the density and/or type of  $\text{Ca}^{2+}$  channels on terminals (assuming some basal level of channel activity), consistent with observations made from evoked  $\text{Ca}^{2+}$  influx in the crayfish NMJ<sup>7</sup> and mammalian CNS terminals.<sup>25</sup> The  $\text{Ca}^{2+}$  sensitivity of release mechanisms could also differ between terminals.<sup>3</sup> An important caveat is that MSCT imaging in the current experiments does not sample AMPA receptors. Therefore, these results must be considered preliminary; information about AMPA receptor mediated miniature events must be obtained in order to rule out the possibility that the low frequency and inactive synapses contain solely AMPA receptors. Work in our laboratory is currently addressing this question.

Our imaging method allows spontaneous miniature release rates to be compared at different synapses on the same dendrite; however, it does not permit measurement of release probability under action potential-evoked conditions. Certain agents have been reported to differentially regulate miniature release rate and evoked release probability,<sup>15,23,46</sup> indicating some expected divergence amongst release mechanisms. Although this is a potential limitation, a large body of evidence suggests that miniature and evoked release probabilities are regulated in parallel at presynaptic terminals. For example, changes in evoked release probability following short-term<sup>50</sup> and long-term<sup>2,28</sup> synaptic enhancement are paralleled by changes in miniature release frequency. While parallel regulation of miniature and evoked release does not imply identical mechanism,<sup>23</sup> it does suggest that vesicles for spontaneous miniature and action potential-evoked release are drawn from the same pool and are therefore subject to common mechanisms of regulation.<sup>38</sup>

Results from our laboratory, using imaging of presynaptic vesicular turnover with FM1-43, indicate a significant correlation between miniature frequency and evoked release probability at single cortical neuron synapses.<sup>37</sup> Furthermore these FM 1-43 experiments indicate that the vesicle pool size (a measure of synapse size) as determined by FM1-43 does correlate, albeit weakly ( $r=0.59$ ), with the probability of miniature synaptic activity. The reasons for this discrepancy (in relation to the current study) may be due to the fixation conditions used, as we did not attempt to fix preparations rapidly.<sup>20,21</sup> However, studies of Rosenmund and Stevens<sup>39</sup> suggest that glutaraldehyde fixation does not promote loss of vesicles. Furthermore, other more indirect measures of vesicle pool size such as synapse volume (measured by confocal microscopy) did not reveal a significant correlation with MSCT rate. A conceivable explanation for the discrepancy of the FM1-43 data with the present data is that MSCT imaging provides a more sensitive measure of release frequency than FM1-43 imaging since it can detect synapses that only show single miniature release event. In contrast, our FM1-43 experiments<sup>37</sup> were only able to detect synapses with relatively higher levels of activity (10s–100 release events within

10 min). Alternatively, as MSCT imaging monitors postsynaptic activity, release events may not always successfully activate postsynaptic receptors. A lack of postsynaptic receptor activation would be surprising given that vesicle release is thought to be both rapid and complete.<sup>5</sup> Furthermore, results from MSCT imaging in cultured cortical neurons<sup>47</sup> indicate that when synapses express both AMPA and NMDA responses, each receptor type is activated during repeated trials of transmitter release indicating ready access of transmitter to receptors. However a recent report in chromaffin cells suggests that vesicles are capable of either complete fusion or “kiss and run” transmitter release depending on the concentration of extracellular calcium.<sup>1</sup> Moreover, NMDA and AMPA type glutamate receptors can be differentially distributed among synapses.<sup>17</sup> Therefore, some spines that we find apparently inactive by means of NMDA receptor mediated  $\text{Ca}^{2+}$  influx may potentially constitute a subpopulation of synapses with a strong preference for expressing AMPA type receptors, and would thus be NMDA-“silent”. Further investigation of this interesting problem using immunogold labeling of glutamate receptor subtypes was prevented by an incompatibility with our currently used peroxidase based staining protocol.

Potential limitations of our structural studies include errors in measurement of miniature synaptic activity frequency. These errors would arise from cases where relatively few events are used to calculate frequency. For example, if a synapse showed only three events the coefficient of variation for the frequency measurement would be  $>50\%$  ( $\sqrt{3/3}$ ).

Our results indicate that some synapses can have more than 10-fold higher rates of miniature release than their neighbors

on the same dendrite.<sup>48</sup> It is possible that the rates of release we observe may be artificially elevated at selected synapses when compared to estimates made using other methods.<sup>33</sup> Conceivably, photodynamic damage to presynaptic terminals could account for the difference in release rates between synapses. However, we believe that this is an unlikely scenario (in this system) given that the presynaptic neuron is devoid of calcium indicator and thus would not absorb fluorescent light and be damaged. Yet, it is still possible that (through some undefined mechanism) damage to postsynaptic elements may exacerbate spontaneous presynaptic release. Again this is also unlikely since we do observe profound differences in spontaneous release rates between adjacent synapses that are present on the same dendrite that would be subject to similar levels of damage. Furthermore, analysis of data sets in which synapses with high rates of miniature synaptic activity were excluded did not improve correlation between measures of presynaptic terminal size and release rates.

In summary, we have examined the link between vesicle number and miniature release rate. In contrast to invertebrate studies our findings are largely negative. We suggest potential technical limitations of our study and hope that these might benefit others working in this field.

*Acknowledgements*—Supported by grants from the Medical Research Council of Canada and the EJLB foundation to T.H.M. T.H.M. is a Medical Research Council Scientist. P.J.M. was supported by a Medical Research Council studentship. O.P. was supported by a (HSP-III) scholarship of the DAAD and a UBC University Graduate Fellowship. We thank Hossein Shayan for assistance with figure construction and data analysis.

#### REFERENCES

- Alés E., Tabares L., Poyato J. M., Valero V., Lindau M. and Alvarez de Toledo G. (1999) High calcium concentrations shift the mode of exocytosis to the kiss and run mechanism. *Nat. Cell Biol.* **1**, 40–44.
- Arancio O., Kandel E. R. and Hawkins R. D. (1995) Activity-dependent long-term enhancement of transmitter release by presynaptic  $3',5'$ -cyclic GMP in cultured hippocampal neurons. *Nature* **376**, 74–80.
- Atwood H. L., Karunanithi S., Georgiou J. and Charlton M. P. (1997) Strength of synaptic transmission at neuromuscular junctions of crustaceans and insects in relation to calcium entry. *Invert. Neurosci.* **3**, 81–87.
- Bailey C. H. and Kandel E. R. (1993) Structural changes accompanying memory storage. *A. Rev. Physiol.* **55**, 397–426.
- Bruns D. and Jahn R. (1995) Real-time measurement of transmitter release from single synaptic vesicles. *Nature* **377**, 62–65.
- Calverley R. K. S. and Jones D. G. (1990) Contributions of dendritic spines and perforated synapses to synaptic plasticity. *Brain. Res. Rev.* **15**, 215–249.
- Cooper R. L., Marin L. and Atwood H. L. (1995) Synaptic differentiation of a single motor neuron: conjoint definition of transmitter release, presynaptic calcium signals, and ultrastructure. *J. Neurosci.* **15**, 4209–4222.
- Desmond N. L. and Levy W. B. (1988) Synaptic interface surface area increases with long-term potentiation in the hippocampal dentate gyrus. *Brain. Res.* **453**, 308–314.
- Dobrunz L. E. and Stevens C. F. (1997) Heterogeneity of release probability, facilitation, and depletion at central synapses. *Neuron* **18**, 95–1008.
- Dubin M. W. (1970) The inner plexiform layer of the vertebrate retina: a quantitative and comparative electron microscopic analysis. *J. comp. Neurol.* **140**, 479–506.
- Edwards F. A. (1995) Anatomy and electrophysiology of fast central synapses lead to a structural model for long-term potentiation. *Physiol. Rev.* **75**, 759–787.
- Engert F. and Bonhoeffer T. (1999) Dendritic spine changes associated with hippocampal long-term synaptic plasticity. *Nature* **399**, 66–70.
- Fifkova E., Anderson C. L., Young S. J. and van Harrevald A. (1982) Effect of anisomycin on stimulation-induced changes in dendritic spines of the dentate granule cells. *J. Neurocytol.* **11**, 183–210.
- Forti L., Bossi M., Bergamaschi A., Villa A. and Malgaroli A. (1997) Loose-patch recordings of single quanta at individual hippocampal synapses. *Nature* **388**, 874–878.
- Geppert M., Goda Y., Stevens C. F. and Südhof T. C. (1997) The small GTP-binding protein Rab3A regulates a late step in synaptic vesicle fusion. *Nature* **387**, 810–814.
- Goda Y. and Südhof T. C. (1997) Calcium regulation of neurotransmitter release: reliably unreliable? *Curr. Opin. Cell Biol.* **9**, 513–518.
- Gomperts S. N., Rao A., Craig A. M., Malenka R. C. and Nicoll R. A. (1998) Postsynaptically silent synapses in single neuron cultures. *Neuron* **21**, 1443–1451.
- Greenough W. T., West R. W. and DeVoogd T. J. (1978) Subsynaptic plate perforations: changes with age and experience in the rat. *Science* **202**, 1096–1098.
- Harris K. M., Jensen F. E. and Tsao B. (1992) Three-dimensional structure of dendritic spines and synapses in rat hippocampus (CA1) at postnatal day 15 and adult ages: implications for the maturation of synaptic physiology and long-term potentiation. *J. Neurosci.* **12**, 2685–2705.
- Heuser J. E. and Reese T. S. (1973) Evidence for recycling of synaptic vesicle membrane during transmitter release at the frog neuromuscular junction. *J. Cell Biol.* **57**, 315–344.
- Heuser J. E., Reese T. S., Dennis M. J., Jan Y., Jan L. and Evans L. (1979) Synaptic vesicle exocytosis captured by quick freezing and correlated with quantal transmitter release. *J. Cell Biol.* **81**, 275–300.

22. Hosokawa T., Rusakov D. A., Bliss T. V. P. and Fine A. (1995) Repeated confocal imaging of individual dendritic spines in the living hippocampal slice: evidence for changes in length and orientation associated with chemically induced LTP. *J. Neurosci.* **15**, 5560–5573.
23. Kondo S. and Marty A. (1998) Differential effects of noradrenaline on evoked, spontaneous and miniature IPSCs in rat cerebellar stellate cells. *J. Physiol.* **509**, 233–243.
24. Lisman J. E. and Harris K. M. (1993) Quantal analysis and synaptic anatomy—integrating two views of hippocampal plasticity. *Trends Neurosci.* **16**, 141–147.
25. Mackenzie P. J., Umekiya M. and Murphy T. H. (1996)  $Ca^{2+}$  imaging of CNS axons in culture indicates reliable coupling between single action potentials and distal functional release sites. *Neuron* **16**, 783–795.
26. Mackenzie P. J., Kenner G. S., Prange O., Shayan H., Umekiya M. and Murphy T. H. (1999) Ultrastructural correlates of synaptic function in cultured cortical neurons. *J. Neurosci.* **19**, C13.
27. Maletic-Savatic M., Malinow R. and Svoboda K. (1999) Rapid dendritic morphogenesis in CA1 hippocampal dendrites induced by synaptic activity. *Science* **283**, 1923–1927.
28. Malgaroli A. and Tsien R. W. (1992) Glutamate-induced long-term potentiation of the frequency of miniature synaptic currents in cultured hippocampal neurons. *Nature* **357**, 134–139.
29. Müller W. and Connor J. A. (1991) Dendritic spines as individual neuronal compartments for synaptic  $Ca^{2+}$  responses. *Nature* **354**, 73–76.
30. Moser M. B., Trommald M., Egeland T. and Andersen P. (1997) Spatial training in a complex environment and isolation alter the spine distribution differently in rat CA1 pyramidal cells. *J. comp. Neurol.* **380**, 373–381.
31. Murphy T. H., Baraban J. M., Wier W. G. and Blatter L. A. (1994) Visualization of quantal synaptic transmission by dendritic calcium imaging. *Science* **263**, 529–532.
32. Murphy T. H., Baraban J. M. and Wier W. G. (1995) Mapping miniature synaptic currents to single synapses using calcium imaging reveals heterogeneity in postsynaptic output. *Neuron* **15**, 159–168.
33. Murthy V. N. and Stevens C. F. (1999) Reversal of synaptic vesicle docking at central synapses. *Nat. Neurosci.* **2**, 503–507.
34. Murthy V. N., Sejnowski T. J. and Stevens C. F. (2000) Dynamics of dendritic calcium transients evoked by quantal release at excitatory hippocampal synapses. *Proc. Natl. Acad. Sci. USA* **97**, 901–906.
35. Papa M. and Segal M. (1996) Morphological plasticity in dendritic spines of cultured hippocampal neurons. *Neuroscience* **71**, 1005–1011.
36. Pierce J. P. and Lewin G. R. (1994) An ultrastructural size principle. *Neuroscience* **58**, 441–446.
37. Prange O. and Murphy T. H. (1999) Correlation of miniature synaptic activity and evoked release probability in cultures of cortical neurons. *J. Neurosci.* **19**, 6427–6438.
38. Rosenmund C. and Stevens C. F. (1996) Definition of the readily releasable pool of vesicles at hippocampal synapses. *Neuron* **16**, 1197–1207.
39. Rosenmund C. and Stevens C. F. (1997) The rate of aldehyde fixation of the exocytotic machinery in cultured hippocampal synapses. *J. Neurosci. Meth.* **76**, 1–5.
40. Rusakov D. A., Davies H. A., Harrison E., Diana G., Richter-Levin G., Bliss T. V. P. and Stewart M. G. (1997) Ultrastructural synaptic correlates of spatial learning in rat hippocampus. *Neurosci.* **80**, 69–77.
41. Schikorski T. and Stevens C. F. (1997) Quantitative ultrastructural analysis of hippocampal excitatory synapses. *J. Neurosci.* **17**, 5858–5867.
42. Shi S.-H., Hayashi Y., Petralia R. S., Zaman S. H., Wenthold R. J., Svoboda K. and Malinow R. (1999) Rapid spine delivery and redistribution of AMPA receptors after synaptic NMDA receptor activation. *Science* **284**, 1811–1816.
43. Sorra K. E. and Harris K. M. (1998) Stability in synapse number and size at 2 hr after long-term potentiation in hippocampal area CA1. *J. Neurosci.* **18**, 658–671.
44. Trommald M., Jensen V. and Andersen P. (1995) Analysis of dendritic spines in rat CA1 pyramidal cells intracellularly filled with a fluorescent dye. *J. comp. Neurol.* **353**, 260–274.
45. Trommald M. and Hüllenberg G. (1997) Dimensions and density of dendritic spines from rat dentate granule cells based on reconstructions from serial electron micrographs. *J. comp. Neurol.* **377**, 15–28.
46. Trudeau L. E., Doyle R. T., Emery D. G. and Haydon P. G. (1996) Calcium-independent activation of the secretory apparatus by ruthenium red in hippocampal neurons: a new tool to assess modulation of presynaptic function. *J. Neurosci.* **16**, 46–54.
47. Umekiya M., Senda M. and Murphy T. H. (1999) Behavior of NMDA and AMPA receptor mediated miniature excitatory synaptic currents at synapses identified by calcium imaging. *J. Physiol. (Lond.)* **521**, 113–122.
48. Wang S., Prange O. and Murphy T. H. (1999) Amplification of calcium signals at dendritic spines provides a method for CNS quantal analysis. *Can. J. Pharmac. Physiol.* **77**, 651–659.
49. Wojtowicz J. M., Marin L. and Atwood H. L. (1994) Activity-induced changes in synaptic release sites at the crayfish neuromuscular junction. *J. Neurosci.* **14**, 3688–3703.
50. Zucker R. S. (1996) Exocytosis: a molecular and physiological perspective. *Neuron* **17**, 1049–1055.

(Accepted 17 February 2000)